energy&fuels

Article

pubs.acs.org/EF

Removal of Gaseous Elemental Mercury by Cylindrical Activated Coke Loaded with CoO_x-CeO_2 from Simulated Coal Combustion Flue Gas

Huiyu Wu,[†,‡] Caiting Li,[*,†,‡] Lingkui Zhao,[†,‡] Jie Zhang,[†,‡] Guangming Zeng,[†,‡] Yin'e Xie,[†,‡] Xunan Zhang,[†,‡] and Yan Wang[†,‡]

[†]College of Environmental Science and Engineering, Hunan University, Changsha 410082, PR China

[‡]Key Laboratory of Environmental Biology and Pollution Control (Hunan University), Ministry of Education, Changsha 410082, PR China

Supporting Information

ABSTRACT: Co−Ce mixed oxides were loaded on commercial cylindrical activated coke granules (CoCe/AC) by an impregnation method to remove gaseous elemental mercury (Hg^0) from simulated coal combustion flue gas at low temperature (110−230 °C). Effects of the Co/Ce molar ratio in Co−Ce mixed oxides, mixed oxides loading value, reaction temperature, and flue gas components (O_2, NO, SO_2, H_2O) on Hg^0 removal efficiency were investigated, respectively. Brunauer−Emmett−Teller analysis, X-ray diffraction, scanning electron microscopy, Fourier transform infrared spectroscopy, thermogravimetric analysis (TGA), and X-ray photoelectron spectroscopy (XPS) analysis were employed to analyze the characteristics of the samples. Results showed that up to 92.5% of Hg^0 removal efficiency could be obtained over $Co_{4.5}Ce_6$/AC at 170 °C. The remarkably high Hg^0 removal ability of $Co_{4.5}Ce_6$/AC mainly depended on the synergetic effect between cobalt oxide and ceria. Additionally, different with the pure N_2 condition, the existence of O_2 and NO could increase Hg^0 removal efficiency. SO_2 exhibited an inhibitive effect on Hg^0 removal in the absence of O_2. H_2O(g) could slightly hinder Hg^0 removal. The characterization results exhibited that addition of cobalt oxide led to the excellent dispersity of CeO_2 on AC. TGA and XPS analysis results revealed that the captured mercury species on the used $Co_{4.5}Ce_6$/AC mainly existed as HgO, and both lattice oxygen and chemisorption oxygen contributed to Hg^0 oxidation. Furthermore, the mechanisms involved in Hg^0 removal were identified.

1. INTRODUCTION

Mercury (Hg) emission from coal combustion has attracted increasing attention due to its high volatility, persistence, bioaccumulation, and neurological toxicity.[1,2] According to the report of 2010 statistics, the global anthropogenic mercury emission reached 2.320×10^6 kg/a.[3] The coal-fired power plant, which contributed approximately one-third of the global mercury emission, has been considered to be the largest anthropogenic source of mercury emission in the United States.[4−6] Many countries have taken efforts to reduce the mercury emissions in recent years. On December 16, 2011, the U.S. Environmental Protection Agency (EPA) finalized the first ever national standards to reduce mercury and other toxic air pollution from coal and oil-fired power plants.[7] In China, where the coal consumption is the largest in the world,[8] mercury pollution from coal combustion is an important environmental problem; the government issued the Emission Standard of Air pollution for Thermal Power Plants (GB 13223-2011), limiting the mercury emission from coal-fired power plants to 0.03 mg/m^3.[9] In order to implement these stringent mercury control regulations, effective control technologies for mercury removal are urgently needed.

Mercury removal efficiency greatly depends on its forms in postcombustion flue gas. Mercury in coal combustion flue gas generally presents in three forms: elemental (Hg^0), oxidized (Hg^{2+}), and particle-bound (Hg^p).[10,11] The Hg^{2+} and Hg^p can be effectively removed by existing air pollution control devices (APCDs), such as wet flue gas desulfurization (WFDG), fabric filter (FF), or electrostatic precipitations (ESPs). Conversely, Hg^0 is the most difficult to be directly removed by APCDs by virtue of its high volatile, stability, and low water solubility.[12,13] As a result, development of viable technology for effective removal of Hg^0 from flue gas is the primary objective and task of mercury control. Currently, activated carbon injection technology is one of the major commercially available technologies for Hg control from coal-fired power plants, especially activated carbon modified by sulfur, chloride, or iodine.[14,15] But its widespread commercial application is limited due to its high operating cost, poor capacity, low utilization rate, and negative effect on the quality of fly ash as a concrete extender.[16,17] So it is vital to develop novel commercially available materials to improve the operating performance and meanwhile reduce the operating cost of the system for controlling mercury emissions from coal combustion flue gas.

Activated coke (AC) is a kind of porous activated carbon-based adsorbent which is not adequately activated or destructively distilled. Compared with conventional activated carbon, first, AC supports could effectively resist abrasion and crushing during the operation and circulation process due to its higher mechanical strength and better regeneration perform-

Received: April 20, 2015
Revised: September 1, 2015
Published: September 1, 2015

ACS Publications © 2015 American Chemical Society

DOI: 10.1021/acs.energyfuels.5b00871
Energy Fuels 2015, 29, 6747−6757

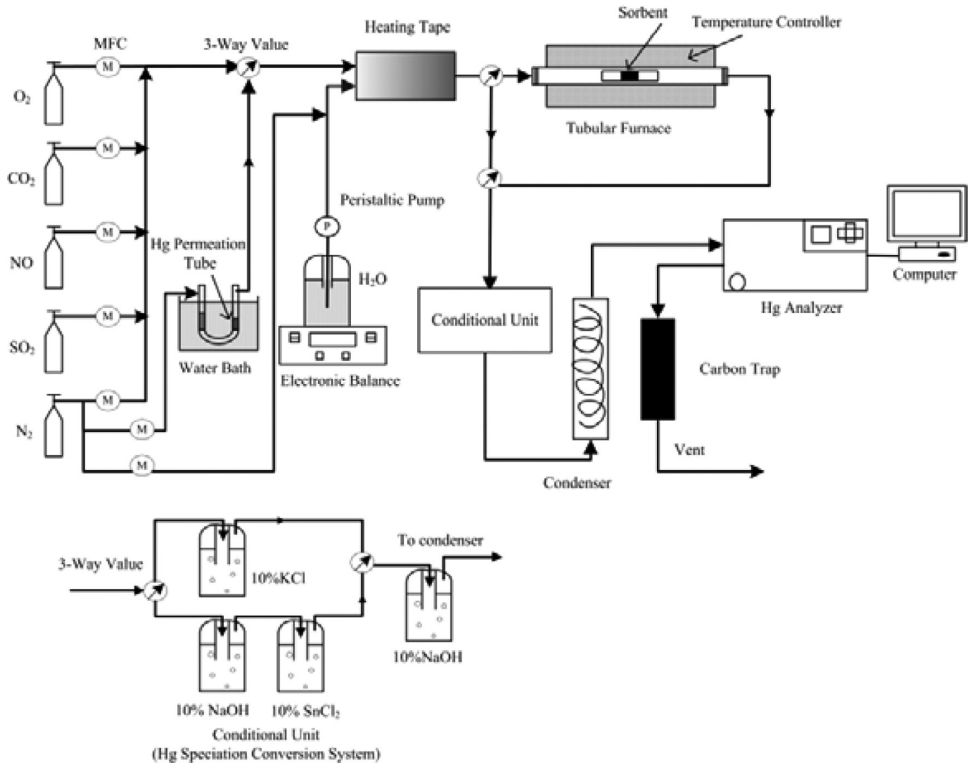

Figure 1. Schematic diagram of the experimental setup.

ance, which will reduce the amount of activated coke that is needed during the Hg control process. Second, AC is commercially available for industrial desulfurization, and it has been reported to be effective for simultaneous removal of SO_2, NO_x, and Hg^0 from flue gas at temperatures below 200 °C,[18,19] which would not only reduce the equipment and operation costs, but also warrant higher boiler efficiencies. Third, the price of activated coke is much lower than that of activated carbon. These advantages grant AC-base technologies promising prospects in industrial applications for Hg^0 control. AC has been proved to have excellent stability in Hg^0 removal,[20] but virgin AC shows poor Hg^0 removal ability. It has been reported that modified AC with metal oxides or chlorides, or treated AC with different acids, can improve the Hg^0 removal capacity of AC.[20−24] Mercury capture using metal oxides has received tremendous attention because of the low cost and environmental friendliness of metal oxide catalysts. CeO_2 is active for the Hg^0 oxidation due to its large oxygen storage capacity and unique redox couple Ce^{3+}/Ce^{4+}. Within the redox shift between Ce^{3+} and Ce^{4+}, labile oxygen vacancies and bulk oxygen species with high mobility can be generated.[21,25,26] Moreover, the combination of CeO_2 with other metal oxides often affects the mobility of oxygen on their surface, and the oxidation state of the element that is combined, which would effectively affect the elements' redox ability.[27] Besides, cobalt-base catalysts have been found to have high activity for Hg^0 oxidation. Mei et al.[28] presented that loading of Co_3O_4 could increase Hg^0 oxidation ability of activated carbon, and the spent sorbent could be regenerated through heating at 673 K under N_2 atmosphere. Liu et al.[29] found that the Co/TiO_2 catalyst showed high Hg^0 oxidation activities within the temperature range of 120−330 °C. Zhang et al.[30] found that the presence of CoO_x led to a better dispersion and more amorphous species of MnO_x and rendered $Co_6Mn_{30}Ti$ a better Hg^0 oxidation ability. Due to the synergistic effect of active Co-base and high oxygen storage-release ceria, Co_3O_4/CeO_2 catalyst and Co_3O_4−CeO_2 composite had been reported as superior catalysts for low temperature CO oxidation,[31−33] methane oxidation,[34,35] and N_2O decomposition.[36] However, Co−Ce mixed oxides supported on cylindrical activated coke granular (CoCe/AC) by the impregnation method for Hg^0 removal have not been reported.

This study investigated the performance of CoCe/AC on Hg^0 removal from simulated coal combustion flue gas at 110−230 °C. The effects of Co/Ce molar ratio of Co−Ce mixed oxide, mixed oxides loading value, reaction temperature and flue gas components on Hg^0 removal efficiency were analyzed. Meanwhile, essential analysis and characterizations of the catalyst-sorbents have been conducted; the synergic effect between cobalt oxide and ceria as well as the mechanism involved in Hg^0 removal was investigated.

2. MATERIALS AND METHODS

2.1. Samples Preparation. The commercial AC (cylindrical granule with diameter of 5 mm and length of 7−10 mm) was obtained from Inner Mongolia KeXing Carbon Industry Co. Ltd., and the virgin AC was washed with deionized (DI) water and subsequently dried in an electric blast oven at 105 °C for 12 h.

The catalyst-sorbents were synthesized by impregnation method using cobalt nitrate ($Co(NO_3)_2{\cdot}6H_2O$) (AR, Tianjin Kemiou, China) and/or cerium nitrate ($Ce(NO_3)_3{\cdot}6H_2O$) (AR, Tianjin Kemiou, China) aqueous solution as precursors and activated coke as support. Co/AC and Ce/AC were prepared by the thermal decomposition of ($Co(NO_3)_2{\cdot}6H_2O$) and ($Ce(NO_3)_3{\cdot}6H_2O$) loaded on AC, respectively. The Co_xCe_y/AC (where "x" refers to the Co/Ce molar ratio in Co−Ce mixed oxides; "y" refers to total metal oxides mass percentage (M/(M+AC), M = Co- and/or Ce- oxide)) were prepared by thermal decomposition of ($Co(NO_3)_2{\cdot}6H_2O$) and ($Ce(NO_3)_3{\cdot}6H_2O$) mixture loaded on AC. In order to identify the effect of Co/Ce molar ratio in Co−Ce mixed oxides on Hg^0 adsorption capacity and physiochemical

DOI: 10.1021/acs.energyfuels.5b00871
Energy Fuels 2015, 29, 6747−6757

Table 1. Experimental Conditions

	experiments and sorbents	flue gas components	temperature (°C)
Set I	Co_xCe_{10}/AC, Co_{10}/AC, Ce_{10}/AC	6% O_2, 12% CO_2, 300 ppm of NO, 400 ppm of SO_2	140
Set II	$Co_{4.5}Ce_2$/AC, $Co_{4.5}Ce_4$/AC, $Co_{4.5}Ce_6$/AC, $Co_{4.5}Ce_8$/AC, $Co_{4.5}Ce_{10}$/AC	6% O_2, 12% CO_2, 300 ppm of NO, 400 ppm of SO_2	110, 140, 170, 200, 230
Set III	$Co_{4.5}Ce_6$/AC	$N_2/(N_2 + O_2)$ + individual flue gas component (NO, SO_2), SFG, SFG (8% H_2O)	170

properties, the nitrates were mixed according to different Co/Ce molar ratios (x) (x = 1, 1.5, 2, 3, 4.5, 6, 9) with y = 10 wt %, and dissolved in deionized water to form the corresponding solution. To further analyze the effect of metal oxides loading value on Hg^0 removal efficiency, AC was impregnated by the mixed nitrate solution corresponding to different concentration (y = 0, 2, 4, 6, 8, 10 wt %) with x = 4.5 for 24 h. After impregnation, the impregnated samples were dried in an electric oven at 105 °C for 12 h and then were calcined at 450 °C under N_2 atmosphere for 4 h.

2.2. Mercury Adsorption and Oxidation Test. The apparatus for performing of catalyst-sorbents' adsorption and oxidation for Hg^0 experiment is shown in Figure 1. The fixed-bed reactor was a quartz tube (with inner diameter of 60 mm and 95 cm in length) placed horizontally in a tubular electric furnace to keep the catalyst-sorbents bed at the desired temperature. The modified activated coke was first loaded in a small quartz tube with an inner diameter of 52 mm and 20 cm in length, the two ends of the bed are compacted with quartz plug, and the small quartz tube was wrapped with an alkali-free band and then loaded into the fixed-bed reactor. The elemental mercury permeation tube (VICI Metronics, USA) was placed in a U-shaped quartz tube which was immersed in a water bath with a constant temperature of 60 °C, and a flow of pure N_2 (200 mL/min) that was used as carrier gas passed through the Hg^0 permeation tube and then gas-phase Hg^0 was generated. In our previous work,[24] the quartz tube and the Teflon tube were proven to have good chemical resistance and inertness properties toward Hg^0. The simulated coal combustion flue gas (denoted as "SFG") used in the experiments was a mixture of Hg^0 (~105 $\mu g/m^3$), 6% O_2, 12% CO_2, 300 ppm of NO, 400 ppm of SO_2, 8% H_2O(g) (when used) and balanced gas N_2. Water vapor was generated by using a peristaltic pump to transfer water into Teflon tube that wrapped with temperature-controlled heating band and the temperature was maintained at 110 °C. A flow of 100 mL/min heated N_2 took the H_2O (g) alone and mixed with flue gas. The total flow rate of the flue gas was 1L/min and accurately controlled by mass flow controllers, the corresponding gas hourly space velocity (GHSV) was approximately 5.0×10^3 h^{-1}. All of the gases were sufficiently mixed before passing into the reactor.

The experimental conditions are summarized in Table 1. In each test, about a 18 g sample was packed in the middle of the fixed-bed reactor. The inlet and outlet Hg^0 concentration were measured by RA-915M online mercury analyzer (LUMEX, Russia) with a detection limit of 2 ng/m^3, which could measure the concentration of Hg^0. A mercury speciation conversion system coupled with RA-915M mercury analyzer was employed to measure Hg^0 and Hg^{2+} concentrations in the outlet flue gas when it necessary. The specifications of the mercury speciation conversion system are described in the Supporting Information. The mercury-laden gas stream was first bypassed the reactor and passed through the RA-915M online mercury analyzer until inlet Hg^0 concentration (Hg^0_{in}) was stable. Once thermal stability was reached, the gas flow was diverted to pass through the fixed-bed reactor and maintained for 3 h. At the end of each test, the mercury analyzer was switched to the inlet of the reactor to verify the Hg^0_{in} again. Water vapor was removed by a condenser before accessing to the mercury analyzer. The total Hg^0 removal efficiency (E_{rem}) can be defined as

$$E_{rem}(\%) = \frac{Hg^0_{in} - Hg^0_{out}}{Hg^0_{in}} \quad (1)$$

The Hg^0_{in} and Hg^0_{out} represent the Hg^0 concentration ($\mu g/m^3$) at the inlet and outlet of the reactor, respectively.

2.3. Samples Characterization. *2.3.1. Brunauer–Emmett–Teller (BET).* The Brunauer-Emmett–Teller (BET) specific surface area and pore size distribution of the samples were determined by nitrogen adsorption on a TriStar II 3020 analyzer (Micromeritics Instrument Corp, USA). Each sample was degassed in a vacuum at 120 °C for 5 h. The specific surface areas were calculated by the BET method. The average pore diameter and average pore volume were obtained from the desorption branches of N_2 adsorption isotherm and calculated by the Barrett–Joyner–Halenda (BJH) formula.

2.3.2. X-ray Diffraction (XRD). The X-ray diffractogram measurements were carried out on Siemens D5000 powder diffractometer operating at 35 Kv and 30 mA, and using nickel-filter Cu Kα radiation to determine the crystal structure and dispersity of the sorbents. The scanning range was from 10° to 80° with a step size of 2°/min.

2.3.3. Scanning Electron Microscopy (SEM). To further analyze the properties of the sorbents, the morphology and surface structure of the samples were observed by using scanning electron microscopy (SEM) on S-4800 (Hitachi, Japan).

2.3.4. Fourier Transforms Infrared (FTIR) Spectroscopy. Fourier transform infrared (FTIR) spectroscopy was recorded on a FTIR-8400S IRprestige-21 (Shimadzu, Japan) spectrometer to qualitatively measure the surface groups of the samples. The spectral region between 4000 and 400 cm^{-1} was scanned with a 2 cm^{-1} resolution. Before the analysis, the samples were grinded and then mixed with KBr (SP, Sinopharm, China) in a ratio of 1:100 of a sample to KBr.

2.3.5. X-ray Photoelectron Spectroscopy (XPS). X-ray photoelectron spectroscopy (XPS) analysis was conducted on a K-Alpha 1063 X-ray photoelectron spectrometer (Thermo Fisher Scientific, USA) using 72W Al Kα radiation from micro aggregation monochromator. Before the XPS characterization analysis, the sample had to undergo two levels of vacuum pretreatment in order to obtain a detection environment with a very high vacuum degree. First, the samples were degassed for about 2 h in a prevacuum chamber reaching a vacuum degree of 5×10^{-2} mPa, and then the samples were transferred to analysis chamber and degassed for about 3 h reaching a vacuum degree of 3×10^{-8} mPa. The binding energies were calibrated by C 1s (284.6 eV).

2.3.6. Thermogravimetric Analysis. The thermogravimetric analysis (TGA) was performed with DTG-60 thermal analyzer (Shimadzu, Japan) to evaluate the thermal stability of the mercury species formed on AC. Approximately 10 mg sample was used and heated from room temperature to 600 °C with a heating rate of 10 °C/min under N_2 atmosphere at a flow rate of 50 mL/min.

3. RESULTS AND DISCUSSION

3.1. Mercury Removal Performance. *3.1.1. Effect of Co/Ce Molar Ratio.* The effect of Co/Ce molar ratio of Co_xCe_{10}/AC on Hg^0 removal was studied. As shown in Figure 2, the Co_xCe_{10}/AC possessed a better Hg^0 removal ability than Co_{10}/AC and Ce_{10}/AC, indicating that a synergistic effect existed between cobalt oxide and ceria in Co_xCe_{10}/AC, as adding CeO_2 could lead to an increase in the amount of reducible Co^{3+} and improve the redox ability of Co^{2+}/ Co^{3+} by facilitating the mobility of adsorbed oxygen species,[34,36] which could enhance the Hg^0 removal efficiency. What is more, the Hg^0 removal efficiency first increased with the increase of Co/Ce molar ratio from 1 to 4.5, and then decreased with the Co/Ce ratio further increases to 9, indicating that an addition of suitable amount of CeO_2 was favorable for Hg^0 removal efficiency. As the catalyst-

DOI: 10.1021/acs.energyfuels.5b00871
Energy Fuels 2015, 29, 6747–6757

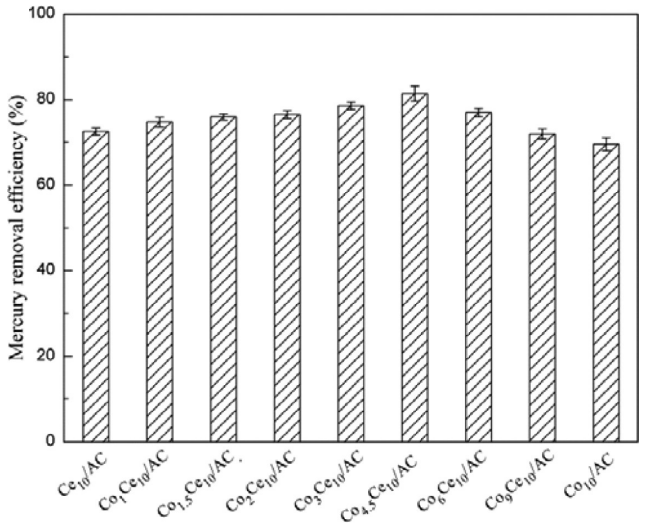

Figure 2. Effect of different Co/Ce molar ratios (x) on Hg^0 removal efficiency over Co_xCe_{10}/AC. (Reaction condition: Hg^0 (~105 $\mu g/m^3$), 6% O_2, 12% CO_2, 300 ppm of NO, 400 ppm of SO_2, and balance gas N_2, 1L/min, GHSV = 5000h^{-1}, T = 170 °C.)

sorbent with Co/Ce molar ratio of 4.5 exhibited the best Hg^0 removal ability, further studies were conducted on the $Co_{4.5}Ce_y$/AC.

3.1.2. Effects of Loading Value and Reaction Temperature. The Hg^0 removal performances over virgin AC and $Co_{4.5}Ce_y$/AC at 110−230 °C under SFG condition were investigated. As shown in Figure 3, all of $Co_{4.5}Ce_y$/AC exhibited better Hg^0

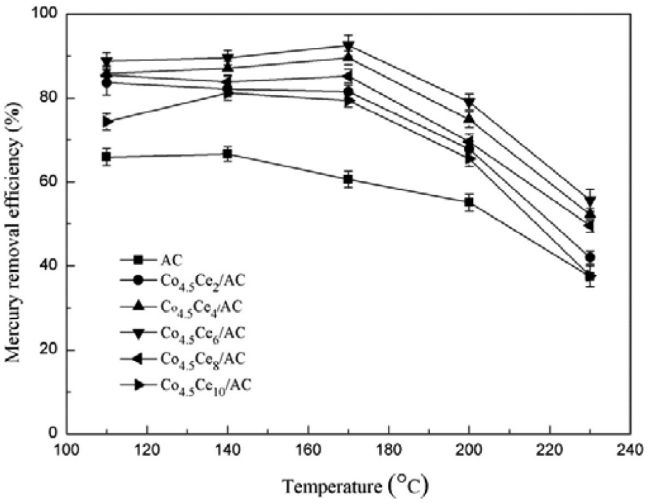

Figure 3. Effects of loading value and reaction temperature on Hg^0 removal efficiency of $Co_{4.5}Ce_y$/AC. (Reaction condition: Hg^0 (~105 $\mu g/m^3$), 6% O_2, 12% CO_2, 300 ppm of NO, 400 ppm of SO_2, and balance gas N_2, 1L/min, GHSV = 5000 h^{-1}.)

removal ability than virgin AC, and the $Co_{4.5}Ce_6$/AC exhibited the best Hg^0 removal ability among all the samples at the temperature of 110−230 °C. Too small amount oxides loading would supply insufficient active sites for Hg^0 removal, but excessive oxides loading may cause the decrease in the specific surface area and the dispersity of mixed oxides on the surface of AC, which might be the reasons for the decrease in Hg^0 removal efficiency. For the Co−Ce mixed oxides modified AC with different loading values, the order of the Hg^0 removal efficiency was as follows: 6 wt % > 4 wt % > 8 wt % > 2 wt % > 10 wt % > 0 wt %, which was not in accordance with the trend of the BET specific surface area, implying that Hg^0 removal efficiency of $Co_{4.5}Ce_y$/AC was attributed to the combination effect of adsorption and oxidation.

Additionally, since chemical adsorption rates and reaction rates generally increase as temperature increased, the Hg^0 removal efficiency first increased along with the increase of reaction temperature from 110 to 170 °C, but the sustained growth of reaction temperature to 230 °C would lead to a decrease in it. This phenomenon was likely a result of the inhibition of the physisorption of Hg^0 which was crucial to Hg^0 removal, as well as the desorption of the adsorbed HgO at the higher temperature.[30] The maximum Hg^0 removal efficiency of about 92.5% could be obtained over $Co_{4.5}Ce_6$/AC at 170 °C. These results manifested that Hg^0 removal over $Co_{4.5}Ce_6$/AC was influenced by temperature, and a proper reaction temperature was beneficial for Hg^0 removal. Therefore, $Co_{4.5}Ce_6$/AC and the optimal reaction temperature (170 °C) were selected as default operational conditions in the following experiments.

According to the Supporting Information, it can be found that Hg^{2+} and Hg^0 were coexisted in the outlet flue gas, and a portion of mercury were captured on the $Co_{4.5}Ce_6$/AC. The results verified that Hg^0 removal efficiency of $Co_{4.5}Ce_6$/AC resulted from the adsorption and catalytic oxidation of Hg^0.

3.2. Samples Characteristics. *3.2.1. BET Analysis.* The BET specific surface area, pore volumes, and average pore diameters of the samples are listed in Table 2. It can be

Table 2. BET Specific Surface Area and Pore Parameters of the Samples

sample	specific surface area (m^2/g)	pore volume (cm^3/g)	average pore size (nm)
AC	295	0.143	1.94
$Co_{4.5}Ce_2$/AC	284	0.143	2.01
$Co_{4.5}Ce_4$/AC	281	0.146	2.08
$Co_{4.5}Ce_6$/AC	281	0.150	2.07
$Co_{4.5}Ce_{10}$/AC	280	0.162	2.31
Co_6/AC	290	0.168	2.31
Ce_6/AC	281	0.135	1.92

observed that the virgin AC possessed the highest specific surface area of 295 m^2/g, however, after loading with cobalt oxide and/or ceria on AC support, the BET specific surface area distinctly dropped with increasing of the mixed oxides content. This indicated that Co−Ce mixed oxides mainly dispersed on the external surface of the support, and excessive metal oxides loading would result in agglomeration and blocking the internal micropore of AC. However, the pore volume and averaged pore size moderately increased to a certain extent except Ce_6/AC. This can be explained by taking the pore size distribution into consideration, as pore volume characteristic is determined primarily by macropore and mesopore, with ascopore and micropore as auxiliary.[37] And partial thin pore walls may be damaged by interaction between Co−Ce mixed oxides and AC.[20]

3.2.2. XRD Analysis. The XRD patterns of virgin AC, Co_6/AC and Ce_6/AC, and series of $Co_{4.5}Ce_y$/AC are shown in Figure 4. The crystalline phases were identified by comparison with Joint Committee Powder Diffraction Standards (JCPDSs). For virgin AC, two strong diffraction peaks attributed to AC

DOI: 10.1021/acs.energyfuels.5b00871
Energy Fuels 2015, 29, 6747−6757

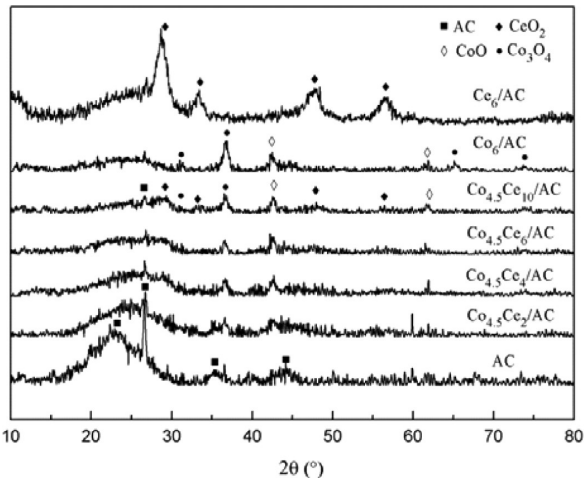

Figure 4. XRD patterns of virgin AC, $Co_{4.5}Ce_2$/AC, $Co_{4.5}Ce_4$/AC, $Co_{4.5}Ce_6$/AC, $Co_{4.5}Ce_{10}$/AC, Co_6/AC and Ce_6/AC.

were detected at 2θ = 26.603°, 44.464° (JCPDS 25-0284). However, the intensity of these peaks decreased or even disappeared with the increase of Co−Ce mixed oxides content, suggesting that there was interaction between the Co−Ce mixed oxides and AC. The diffraction peaks at 2θ = 31.249°, 36.836°, 65.220°, 74.076° (JCPDS 09-0418) in Co_6/AC belonged to Co_3O_4, and the peaks at 42.387° and 61.496° (JCPDS 48-1719) were ascribed to CoO. This indicated that Co_3O_4 and CoO were coexisted on the Co_6/AC, and cobalt species were predominantly in the form of Co_3O_4, which is more active for Hg^0 oxidation.[29] In Ce_6/AC, the visible diffraction peaks at 2θ = 28.549°, 33.077°, 47.489°, and 56.326° (JCPDS 04-0593) corresponding to CeO_2. For $Co_{4.5}Ce_y$/AC, the Co species and Ce species mainly existed as Co_3O_4 and CeO_2, respectively. And no phase containing both Co and Ce was observed, which indicated that there were no Co−Ce composite oxides on the surface of $Co_{4.5}Ce_y$/AC. In comparing with the XRD patterns of Ce_6/AC and Co_6/AC, the peaks of CeO_2 and Co_3O_4 on $Co_{4.5}Ce_y$/AC became much weaker and broader; moreover, no obvious characteristic peaks for CeO_2 were detected when the Co−Ce mixed oxides loading value was equal or less than 6 wt %, implying the existence of cobalt oxide led to an excellent dispersion of CeO_2 over AC, CeO_2 possibly existed as highly dispersed or amorphous surface species in the $Co_{4.5}Ce_y$/AC,[31,38] which was beneficial for Hg^0 removal.

3.2.3. SEM Analysis. Figure 5 shows the SEM images of the selected samples. It can be seen that the surface morphology of AC was changed by loading with Co−Ce mixed oxides, which were mainly dispersed on the surface of AC. It should be noted that metal oxides on the $Co_{4.5}Ce_6$/AC had the best dispersity among the samples, and only a few agglomerates were observed, whereas more agglomerates formed on the surface of AC with further increasing in loading value, which was in agreement with the results of the BET test. By combining XRD and SEM characterization results, the highly dispersion of Co−Ce mixed oxides on AC surface was favorable for the outstanding Hg^0 removal efficiency of $Co_{4.5}Ce_6$/AC.

3.2.4. FTIR Analysis. The FTIR spectra of AC and fresh $Co_{4.5}Ce_6$/AC were almost similar (Figure 6). The adsorption peak at 3740 cm^{-1} was ascribed to the stretching vibration of the hydroxyl groups (OH) on the sample's surface or the OH of chemical adsorption,[39] while 1600−1400 and 1361 cm^{-1} regions were ascribed to C═C and C═N groups in the surface of AC,[40] the absorption bands at 1120 to 1040 cm^{-1} corresponding to the phenol, or the C−O, O−C−O bending vibrations.[41] The adsorption peak at near 1660 cm^{-1} was attributed to C═O stretching vibrations, as indicative of carboxyl, carbonyl, and lactones.[1] The results indicated that AC-base catalyst-sorbents contained various functional groups, such as OH, C−O, and C═O groups, which could provide active sites for the physical and chemical adsorption of Hg^0, thus granting virgin AC the Hg^0 removal ability to a certain extent. In addition, loading of Co−Ce mixed oxides on AC by the impregnation method in this study had little influence on the surface functional groups structure of AC support, and we speculated that the remarkably higher Hg^0 removal ability of $Co_{4.5}Ce_6$/AC than AC mainly depended on the high dispersion and the redox property of Co−Ce mixed oxides.

3.2.5. XPS Analysis. XPS analysis was performed to examine the valence states of the elements on the surface of Co_6/AC, Ce_6/AC, the fresh and the used $Co_{4.5}Ce_6$/AC. The O 1s spectra of the samples shown in Figure 7 were fitted in three peaks, including peaks at lower binding energy value 529.4−530.1 eV (assigned to lattice oxygen from the Co−Ce mixed oxides loaded on AC, denoted as O_α), 531.4 eV (assigned to chemisorbed oxygen or/and weakly bonded oxygen, denoted as O_β), (532.5 ± 0.1) eV (assigned to the surface oxygen in hydroxyl species or/and adsorbed water species, denoted as O_γ).[37,42,43] The concentration of O_α, O_β, O_γ of the samples were calculated by O_α /O_T, O_β /O_T, and O_γ /O_T, $O_T = O_\alpha + O_\beta + O_\gamma$, respectively. As summarized in Table 3, the O_β concentration of $Co_{4.5}Ce_6$/AC was higher than that of Co_6/AC and Ce_6/AC, revealing that the combination of cobalt oxide and ceria gave rise to more surface oxygen, which was beneficial for Hg^0 removal.[44] It was noteworthy that the concentration of lattice oxygen was clearly improved after being modified with Ce−Co mixed oxides. Yet the ratio of lattice oxygen on the used $Co_{4.5}Ce_6$/AC declined to 43.7% as compared to the fresh sample (54.5%), and the ratio of O_β decreased from 29.6% to 21.6% as well. These observations revealed that both lattice oxygen and chemisorbed oxygen or/and weakly adsorbed oxygen participated in Hg^0 oxidation.

From the Co 2p spectra of XPS shown in Figure 8, it is apparent that the Co species mainly existed as Co_3O_4 phase (779.7, 781.4, and 796.3 eV) and coupled with CoO (~786.1 eV, 802.7 eV).[45,46] The ratio of Co_3O_4/CoO was improved from 1.25 to 1.55 after the catalyst-sorbent was modified with CeO_2, indicating that an addition of CeO_2 could affect the oxidation state of cobalt, which was related to the oxygen storage-release properties of CeO_2, and some oxygen in ceria was incorporated into cobalt to form higher valence state of cobalt.[33,47] From Figure 8, great changes were observed after the Hg^0 removal process, the peak at 779.7 eV disappeared, and there was a chemical shift toward higher binding energies for Co 2p as compared to the fresh $Co_{4.5}Ce_6$/AC; this fact may result from the interaction between cobalt oxide and ceria during Hg^0 removal process. The peaks shifted to higher binding energy near 782.8 and 798.3 eV belonged to Co_3O_4.[46,48,49] Moreover, the peak area ratio of Co_3O_4/CoO decreased from 1.55 to 0.74 after Hg^0 removal process, and the reduction of Co_3O_4 contributed to Hg^0 oxidation.

The XPS spectra of Ce 3d for Ce_6/AC, the fresh and the used $Co_{4.5}Ce_6$/AC are shown in Figure 9. The peaks labeled as v were assigned to Ce $3d_{5/2}$, and those denoted as u were corresponding to Ce $3d_{3/2}$. The u/v, u_2/v_2, and u_3/v_3 represented the $3d^{10}4f^0$ state of Ce^{4+}, while the doublet labeled

DOI: 10.1021/acs.energyfuels.5b00871
Energy Fuels 2015, 29, 6747−6757

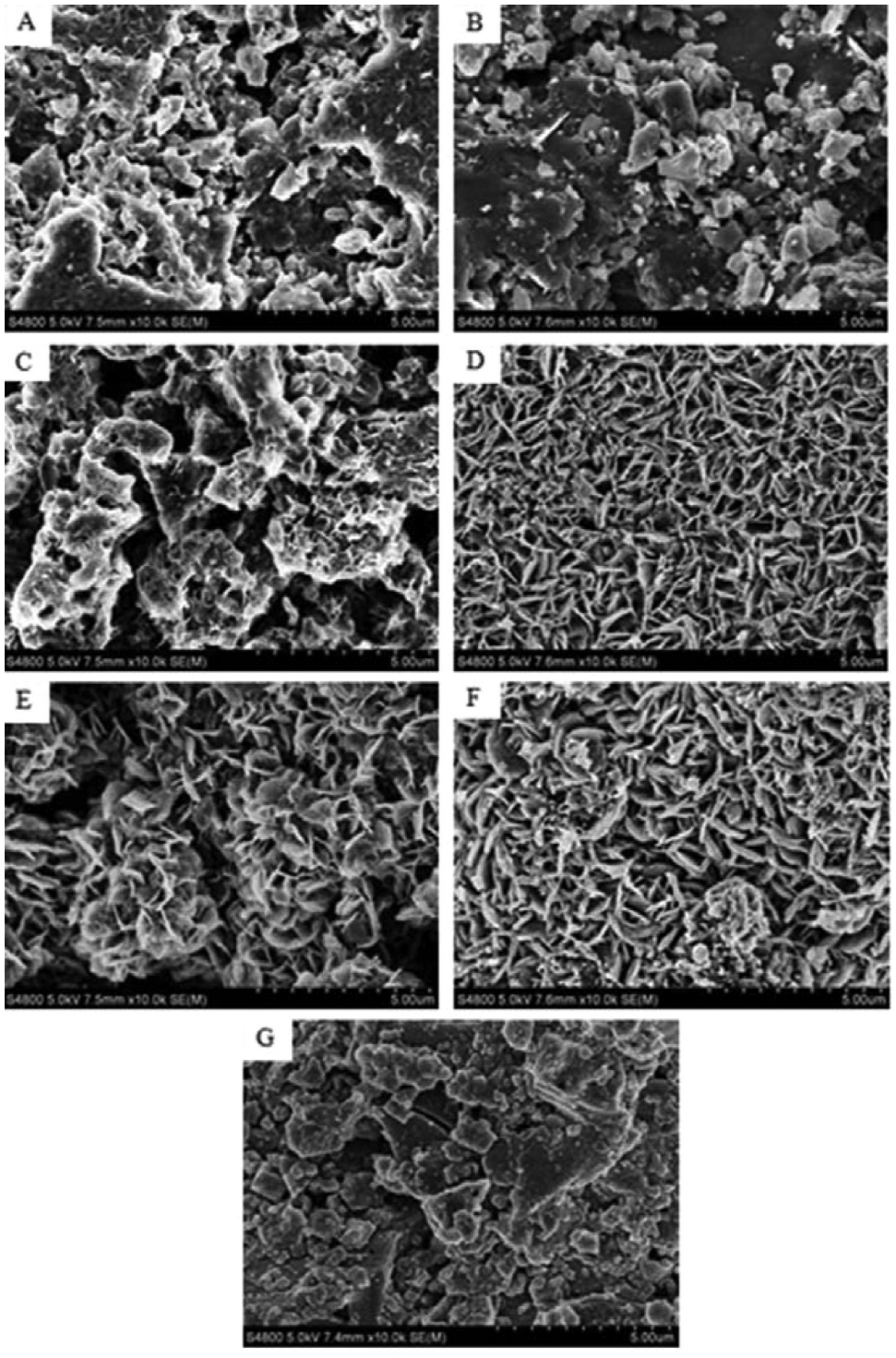

Figure 5. SEM images of (A) virgin AC, (B) $Co_{4.5}Ce_2$/AC, (C) $Co_{4.5}Ce_4$/AC, (D) $Co_{4.5}Ce_6$/AC, (E) $Co_{4.5}Ce_{10}$/AC, (F) Co_6/AC and (G) Ce_6/AC.

u_1/v_1 represented the $3d^{10}4f^1$ initial electronic state corresponding to Ce^{3+}.[43,50] Both Ce^{3+} and Ce^{4+} oxidation states existed on the surface of Ce_6/AC and $Co_{4.5}Ce_6$/AC, and the Ce species were primarily in the form of CeO_2. The peak area ratio of Ce^{4+}/Ce^{3+} had a slightly change from 3.75 to 3.10 when cobalt oxide was introduced, demonstrating that the valence state of Ce ions decreased from Ce^{4+} to Ce^{3+} upon Co doping.[38] The presence of Ce^{3+} species could create charge imbalance, vacancies, and unsaturated chemical bonds on the surface of samples,[51] which was highly active for Hg^0 removal; therefore, the increase in Ce^{3+} concentration would bring about more surface oxygen for Hg^0 removal. Furthermore, the ratio of Ce^{4+}/Ce^{3+} on the used $Co_{4.5}Ce_6$/AC decreased to 1.80, which indicated that CeO_2 on the $Co_{4.5}Ce_6$/AC participated in the Hg^0 removal process.

On the basis of the XRD and XPS analysis, it can be proposed that a synergistic effect existed between cobalt oxide and ceria, which was in accordance with the effect of ceria to maintain a higher valence state of manganese observed by Imamura et al.[27] The combination of cobalt oxide and ceria

DOI: 10.1021/acs.energyfuels.5b00871
Energy Fuels 2015, 29, 6747−6757

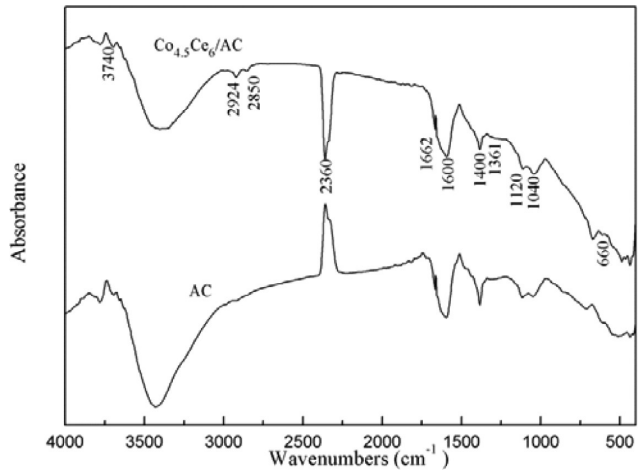

Figure 6. FTIR spectra of (bottom) virgin AC, (top) the fresh $Co_{4.5}Ce_6$/AC.

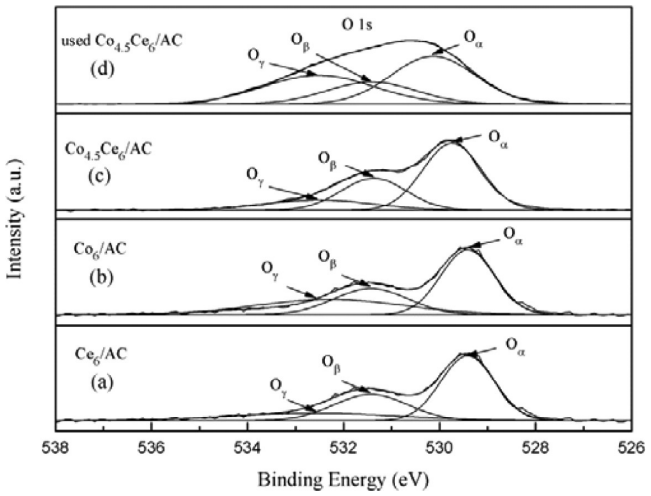

Figure 7. O 1s XPS spectra for Co_6/AC, Ce_6/AC, the fresh and the used $Ce_{4.5}Ce_6$/AC.

Table 3. Concentrations of Different Type Oxygen (O_α, O_β, O_γ) in Co_6/AC, Ce_6/AC, the Fresh and the Used $Co_{4.5}Ce_6$/AC

	concentration of the oxygen		
samples	O_α (%)	O_β (%)	O_γ (%)
Co_6/AC	46.7	28.5	24.8
Ce_6/AC	52.2	29.0	18.8
$Co_{4.5}Ce_6$/AC	54.5	29.6	15.9
used $Co_{4.5}Ce_6$/AC	43.7	21.6	34.7

would make some CeO_2 transform to Ce_2O_3; namely, the valence state of Ce ions decreased from Ce^{4+} to Ce^{3+} upon Co doping and meanwhile make some CoO transform to Co_3O_4, which was related to the oxygen storage-release properties of CeO_2. The possible synergetic mechanism between cobalt oxide and ceria can be explained by the following reactions:

$$Co_3O_4 \rightarrow 3CoO + [O] \quad (2)$$

$$2CeO_2 + 3CoO \rightarrow Ce_2O_3 + Co_3O_4 \quad (3)$$

$$Ce_2O_3 + 1/2O_2 \rightarrow 2CeO_2 \quad (4)$$

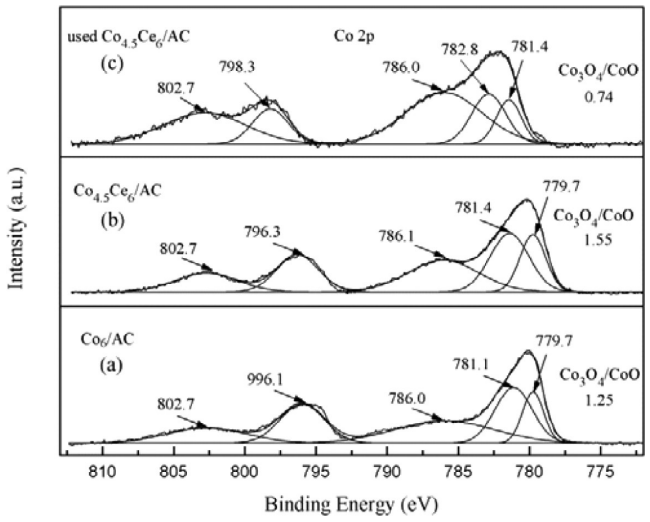

Figure 8. Co 2p XPS spectra for Co_6/AC, the fresh and the used $Ce_{4.5}Ce_6$/AC.

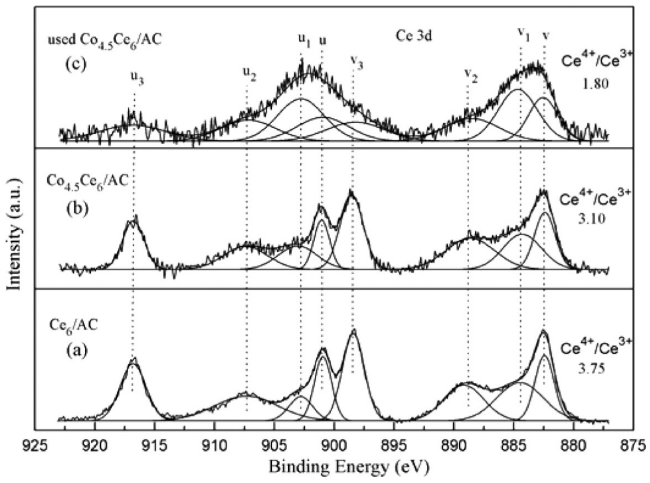

Figure 9. Ce 3d XPS spectra for Ce_6/AC, the fresh and the used $Ce_{4.5}Ce_6$/AC.

The XPS spectrum of Hg 4f of the used $Co_{4.5}Ce_6$/AC is shown in Figure 10. The strong peak at 102.9 eV was ascribed

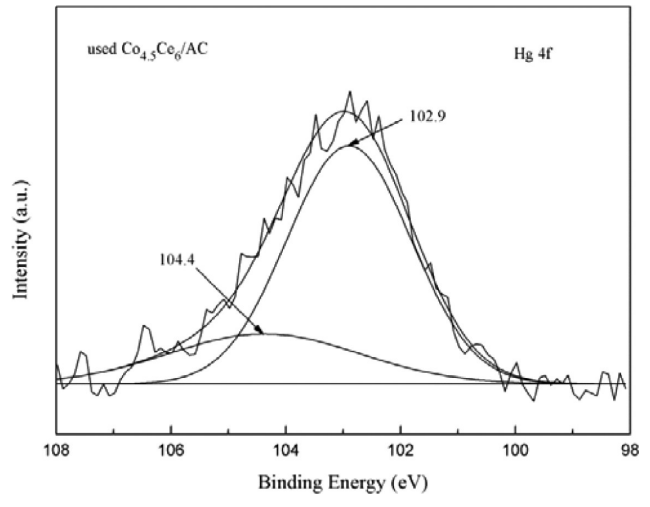

Figure 10. Hg 4f XPS spectra for the used $Ce_{4.5}Ce_6$/AC.

DOI: 10.1021/acs.energyfuels.5b00871
Energy Fuels 2015, 29, 6747−6757

to the Si 2p (SiO_2), which is one of the components of activated coke ash. And the peak at higher biding energy (BE = 104.4 eV) corresponded to the character of Hg $4f_{5/2}$ for HgO.[24] However, no adsorbed Hg^0 was detected on the surface of the sample, which may due to Hg^0 escaping when the sample was treated prior to XPS analysis. On the basis of the XPS spectrum of Hg 4f, it can be deduced that HgO was a major product of Hg^0 removal by $Co_{4.5}Ce_6$/AC at 170 °C under SFG condition.

3.2.6. TGA Analysis. TGA was used to analyze the thermal stability of virgin AC, the fresh $Co_{4.5}Ce_6$/AC, and the used $Co_{4.5}Ce_6$/AC, which were held in the simulated flue gas stream in the absent or present of Hg^0; the adsorbed mercury species on the used $Co_{4.5}Ce_6$/AC were analyzed as well. In Figure 11,

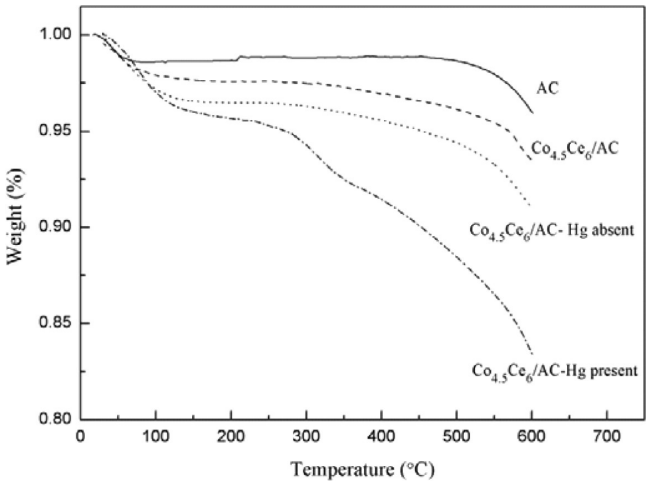

Figure 11. TGA curves of virgin AC, the fresh and the used $Co_{4.5}Ce_6$/AC.

the initial weight loss below 110 °C was generally attributed to the evaporation of adsorbed water. In the temperature range of 110−500 °C, the virgin AC exhibited negligible weight loss, a slight and slow change in fresh $Co_{4.5}Ce_6$/AC and the $Co_{4.5}Ce_6$/AC- Hg absent, which is probably due to the interaction between the Co−Ce mixed oxides and AC, but the weight loss of the $Co_{4.5}Ce_6$/AC- Hg absent was more obvious than that of the fresh $Co_{4.5}Ce_6$/AC. The weight loss of $Co_{4.5}Ce_6$/AC- Hg present during 110−270 °C was very slight, which was similar to that of fresh $Co_{4.5}Ce_6$/AC and $Co_{4.5}Ce_6$/AC- Hg absent. However, the quick weight loss between 270 and 500 °C was mainly attributed to the decomposition of HgO formed and desorption of little amounts of physically adsorbed Hg^0 on the $Co_{4.5}Ce_6$/AC- Hg present,[22,52,53] which was consistent with result of XPS analysis. The reasons causing the weight loss at the temperature over 500 °C were complex, including the decomposition of AC function groups,[54] which was manifested by the blank test of virgin AC. The TGA results implied that the mercury species on the surface of used $Co_{4.5}Ce_6$/AC were mainly in the form of HgO and a little amount of Hg^0.

3.3. Effect of Flue Gas Components. Set III experiments were carried out with $Co_{4.5}Ce_6$/AC at 170 °C to explore the roles of flue gas components (O_2, NO, SO_2, H_2O) in the process of Hg^0 removal. The results are summarized in Figure 12.

3.3.1. Effect of O_2. The Hg^0 removal efficiency over $Co_{4.5}Ce_6$/AC at 170 °C under pure N_2 gas flow was observed as 51.6%, which may be due to the adsorption of Hg^0, as well as the reaction between Hg^0 and limited surface oxygen.[55] After

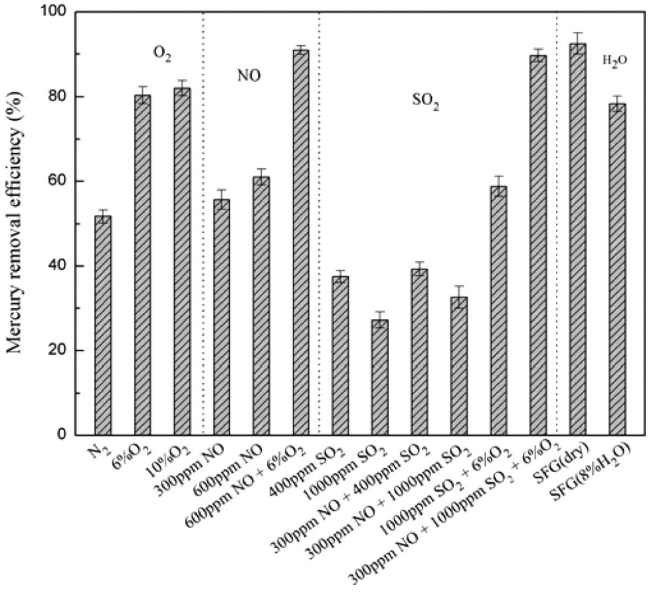

Figure 12. Effects of individual flue gas components on Hg^0 removal efficiency of $Co_{4.5}Ce_6$/AC. (Reaction condition: Hg^0 (~105 $\mu g/m^3$), balance gas N_2, 1L/min, GHSV = 5000h^{-1}, T = 170 °C.)

introducing 6% O_2 into the flue gas, the Hg^0 removal efficiency was greatly improved, whereas no obvious increase in Hg^0 removal efficiency was observed when the O_2 concentration was further increased to 10%. This indicated that O_2 in the flue gas played an important role in Hg^0 oxidation process, but redundant O_2 concentration had little influence on Hg^0 removal. On the basis of the results of characterization analysis and the experiments, it can be speculated that mercury oxidation over $Co_{4.5}Ce_6$/AC mainly follows a Mars-Masson mechanism.[56−58] In this mechanism, Hg^0 first adsorbed on the surface of the $Co_{4.5}Ce_6$/AC and reacted with lattice oxygen to form an adsorbed HgO, which would partly desorb into the gas phase. The gas-phase O_2 could replenish the consumed lattice oxygen ([O]) and chemisorption oxygen and then reoxidized the reduced metal oxides,[59] accordingly gas-phase O_2 is essential to attain higher Hg^0 removal activity over $Co_{4.5}Ce_6$/AC. The redox cycle can be summarized as follows:

$$Hg^0_{(g)} + \text{surface-AC} \rightarrow Hg^0_{(ad)} \quad (5)$$

$$Co_3O_4 \rightarrow 3CoO + [O] \quad (2)$$

$$2CeO_2 + 3CoO \rightarrow Ce_2O_3 + Co_3O_4 \quad (3)$$

$$2CeO_2 \rightarrow [O] + Ce_2O_3 \quad (6)$$

$$[O] + Hg^0_{(ad)} \rightarrow HgO_{(ad)} \quad (7)$$

$$HgO_{(ad)} \rightarrow HgO_{(g)} \quad (8)$$

$$3CoO + 1/2O_2 \rightarrow Co_3O_4 \quad (9)$$

$$Ce_2O_3 + 1/2O_2 \rightarrow 2CeO_2 \quad (4)$$

The overall reaction can be described as

$$Hg^0_{(g)} + 1/2O_{2(g)} \rightarrow HgO_{(g)} \quad (10)$$

3.3.2. Effect of NO. Promotional effect of NO on Hg^0 removal was observed over $Co_{4.5}Ce_6$/AC at 170 °C. Hg^0

DOI: 10.1021/acs.energyfuels.5b00871
Energy Fuels 2015, 29, 6747−6757

removal efficiencies were 55.6% and 61.0% with respect to 300 and 600 ppm of NO concentrations, respectively, which were slightly higher than that under pure N_2. An addition of 6% O_2 into gas stream with 600 ppm of NO further increased the Hg^0 removal efficiency to 90.9%. It has been reported that NO generally adsorbed on the surface of the sorbents and then could be oxidized by labile surface oxygen giving rise to NO_2,[60] and NO_2 was demonstrated to improve the mercury oxidation on the surface of the sorbents.[13,61] The possible mechanism of Hg^0 oxidation in the presence of NO can be depicted in following eq 11 to eq 14. Addition of O_2 into the flue gas not just replenished the surface oxygen that was consumed by NO, but also drive the reaction eq 11, eq 13, and eq 14 to the right, and thus greatly promoted mercury removal. Meanwhile, volatile mercuric compounds (like $Hg(NO_3)_2$) were generated. However, these products were unstable and likely to be volatile at the reaction temperature (170 °C),[62,63] and parts of them may be emitted into the flue gas.

$$NO + 1/2O_2 \rightarrow NO_2 \quad (11)$$

$$Hg^0 + NO_2 \rightarrow HgO + NO \quad (12)$$

$$Hg^0 + 2NO_2 + O_2 \rightarrow Hg(NO_3)_2 \quad (13)$$

$$Hg^0 + 2NO + 2O_2 \rightarrow Hg(NO_3)_2 \quad (14)$$

3.3.4. Effect of SO_2. As can be seen in the Figure 12, in the absence of O_2, the Hg^0 removal process was inhibited by SO_2. With increase of SO_2 concentration from 400 to 1000 ppm, the inhibitory effect was enhanced, while the inhibitory effect was abated by introducing in 300 ppm of NO. The influence of SO_2 on the Hg^0 removal could be analyzed by the following aspects; on the one hand, SO_2 could adsorb on the surface and active sites of the samples, resulting in the competitive adsorption for the similar active sites between SO_2 and Hg^0, and that the affinity between SO_2 and $Co_{4.5}Ce_6$/AC was stronger than that of Hg^0.[64] On the other hand, SO_2 could react with metal oxides on AC and make it ineffective for mercury oxidation. However, when 6% O_2 was added into the flue gas with 1000 ppm of SO_2 alone or coexisted with 300 ppm of NO balanced in N_2, the Hg^0 removal efficiency was enhanced to 58.8% and 89.7%, respectively. This observation demonstrated that Hg^0 removal could be improved by SO_2 with the aid of O_2, which can be further facilitated by NO on account of the promotional effect of NO. Besides, in the presence of O_2, the existence of Ce^{3+} on the $Co_{4.5}Ce_6$/AC lead to charge imbalance which would promote the oxidation of SO_2 to SO_3 by chemisorption oxygen(O*).[65] The produced SO_3 constituted new chemisorption sites for Hg^0 and could further react with Hg^0 to generate $HgSO_4$,[66] as shown in the following reactions:

$$SO_2 + O^* \rightarrow SO_3 \quad (15)$$

$$Hg^0 + SO_3 + O^* \rightarrow HgSO_4 \quad (16)$$

3.3.5. Effect of H_2O. H_2O unavoidably existed in coal combustion flue gas and generally has been reported to have a great effect on the oxidation and removal of Hg^0 over metal oxides based catalysts.[62] An inhibiting effect of H_2O on Hg^0 removal was observed in this study. The addition of 8% H_2O(g) to the gas stream resulted in slightly decline of Hg^0 removal efficiency, which could be interpreted by the competitive adsorption between H_2O(g) and Hg^0 for active sites on $Co_{4.5}Ce_6$/AC.[67] Additionally, the adsorbed H_2O possibly reacted with the SO_3 to generate H_2SO_4, and the formed H_2SO_4 could further react with Co−Ce mixed oxide to form sulfates, such as $CoSO_4$,[57,68] which had adverse effect on Hg^0 removal. However, the Hg^0 removal efficiency under SFG(8% H_2O) condition was still higher than that under pure N_2, which implied that the promotional effects of NO and SO_2 on Hg^0 removal over $Co_{4.5}Ce_6$/AC in the presence of O_2, as demonstrated above, still outweigh the adverse effect of H_2O.

4. CONCLUSIONS

Co−Ce mixed oxides supported on commercial cylindrical activated coke granular (CoCe/AC) were prepared by the impregnation method, and its Hg^0 removal performances were evaluated in a fixed-bed reactor system under simulated coal combustion flue gas conditions at 110−230 °C. Results showed that CoCe/AC catalyst-sorbents possessed better mercury removal ability than virgin AC, Co/AC, and Ce/AC, which was mainly attributed to the significant synergy of cobalt oxide and ceria. A considerably high Hg^0 removal efficiency (>90%) could be obtained at 170 °C by $Co_{4.5}Ce_6$/AC. Besides, O_2 and NO in the flue gas were observed to promote the Hg^0 removal efficiency, SO_2 showed an inhibitory impact in the absence of O_2 on Hg^0 removal, which can be abated by introducing of NO; H_2O(g) could slightly hinder Hg^0 removal. The characterization results showed that loading of Co−Ce mixed oxides resulted in the decrease of BET specific surface area, adding suitable amount of cobalt oxide could lead to excellent dispersion of CeO_2 on AC. The results of XRD and XPS demonstrated that the CeO_2 and Co_3O_4 were the main active components, and coupled with a little amount of Ce_2O_3 and CoO on the surface of the catalyst-sorbents; additionally, electronic transfer existed between cobalt oxide and ceria. TGA and XPS analysis revealed that Hg^0 could be oxidized by the lattice oxygen (generated from the Ce^{4+}/Ce^{3+} and Co^{3+}/Co^{2+} redox couples) and chemisorption oxygen on the surface of $Co_{4.5}Ce_6$/AC and mainly existed in the form of HgO. As demonstrated above, the removal of Hg^0 from coal combustion flue gas by $Co_{4.5}Ce_6$/AC has a promising industrial application prospect. The regenerability and the simultaneous removal of NO_x, SO_2, and Hg^0 performance of the $Co_{4.5}Ce_6$/AC need to be further studied in the future.

■ ASSOCIATED CONTENT

Supporting Information

The Supporting Information is available free of charge on the ACS Publications website at DOI: 10.1021/acs.energyfuels.5b00871.

Details of the mercury speciation conversion system; Table S1. The Hg^0 removal/capture efficiency of Co4.5Ce6/AC (PDF)

■ AUTHOR INFORMATION

Corresponding Author

*Tel.: +86 731 88649216. Fax: +86 731 88649216. E-mail: ctli@hnu.edu.cn; ctli3@yahoo.com.

Notes

The authors declare no competing financial interest.

■ ACKNOWLEDGMENTS

This work was financially supported by the National Natural Science Foundation of China (51278177, 51478173), and the

DOI: 10.1021/acs.energyfuels.5b00871
Energy Fuels 2015, 29, 6747−6757

National High Technology Research and Development Program of China (863 Program, No. 2011AA060803).

REFERENCES

(1) Li, Y. H.; Lee, C. W.; Gullett, B. K. Importance of activated carbon's oxygen surface functional groups on elemental mercury adsorption. *Fuel* **2003**, *82*, 451−457.

(2) Pavlish, J. H.; Hamre, L. L.; Zhuang, Y. Mercury control technologies for coal combustion and gasification systems. *Fuel* **2010**, *89*, 838−847.

(3) Pirrone, N.; Cinnirella, S.; Feng, X.; Finkelman, R. B.; Friedli, H. R.; Leaner, J.; Mason, R.; Mukherjee, A. B.; Stracher, G. B.; Streets, D. G.; Telmer, K. Global mercury emissions to the atmosphere from anthropogenic and natural sources. *Atmos. Chem. Phys.* **2010**, *10*, 5951−5964.

(4) Schoeny, R. *Mercury Study Report to Congress*; NASA, 1996.

(5) Pavlish, J. H.; Sondreal, E. A.; Mann, M. D.; Olson, E. S.; Galbreath, K. C.; Laudal, D. L.; Benson, S. A. Status review of mercury control options for coal-fired power plants. *Fuel Process. Technol.* **2003**, *82*, 89−165.

(6) Pacyna, E. G.; Pacyna, J. M.; Steenhuisen, F.; Wilson, S. Global anthropogenic mercury emission inventory for 2000. *Atmos. Environ.* **2006**, *40*, 4048−4063.

(7) *Final Mercury and Air Toxics Standards (MATS) for Power Plants*; EPA, 2011.

(8) Wang, Q.; Shen, W.; Ma, Z. Estimation of mercury emission from coal combustion in China. *Environ. Sci. Technol.* **2000**, *34*, 2711−2713.

(9) Emission standard of air pollutants for thermal power plants (GB 13223-2011); SEPA: Beijing, 2011.

(10) Galbreath, K. C.; Zygarlicke, C. J. Mercury transformations in coal combustion flue gas. *Fuel Process. Technol.* **2000**, *65−66*, 289−310.

(11) Guo, X.; Zheng, C. G.; Xu, M. Characterization of mercury emissions from a coal-fired power plant. *Energy Fuels* **2007**, *21*, 898−902.

(12) He, S.; Zhou, J. S.; Zhu, Y. Q.; Luo, Z. Y.; Ni, M. J.; Cen, K. F. Mercury Oxidation over a Vanadia-based Selective Catalytic Reduction Catalyst. *Energy Fuels* **2009**, *23*, 253−259.

(13) Norton, G. A.; Yang, H.; Brown, R. C.; Laudal, D. L.; Dunham, G. E.; Erjavec, J. Heterogeneous oxidation of mercury in simulated post combustion conditions. *Fuel* **2003**, *82*, 107−116.

(14) Lee, S. J.; Seo, Y. C.; Jurng, J.; Lee, T. G. Removal of gas-phase elemental mercury by iodine- and chlorine-impregnated activated carbons. *Atmos. Environ.* **2004**, *38*, 4887−4893.

(15) Liu, W.; Vidic, R. D.; Brown, T. D. Impact of flue gas conditions on mercury uptake by sulfur-impregnated activated carbon. *Environ. Sci. Technol.* **2000**, *34*, 154−159.

(16) Lineberry, Q. J.; Cao, Y.; Lin, Y.; Ghose, S.; Connell, J. W.; Pan, W. P. Mercury capture from flue gas using palladium nanoparticle-decorated substrates as injected sorbent. *Energy Fuels* **2009**, *23*, 1512−1517.

(17) Sun, C.; Snape, C. E.; Liu, H. Development of low-cost functional adsorbents for control of mercury (Hg) emissions from coal combustion. *Energy Fuels* **2013**, *27*, 3875−3882.

(18) Olson, D. G.; Tsuji, K.; Shiraishi, I. The reduction of gas phase air toxics from combustion and incineration sources using the MET−Mitsui−BF activated coke process. *Fuel Process. Technol.* **2000**, *65−66*, 393−405.

(19) Tsuji, K.; Shiraishi, I. Combined desulfurization, denitrification and reduction of air toxics using activated coke: 1. Activity of activated coke. *Fuel* **1997**, *76*, 549−553.

(20) Ma, J.; Li, C.; Zhao, L.; Zhang, J.; Song, J.; Zeng, G.; Zhang, X.; Xie, Y. Study on removal of elemental mercury from simulated flue gas over activated coke treated by acid. *Appl. Surf. Sci.* **2015**, *329*, 292−300.

(21) Hua, X.; Zhou, J.; Li, Q.; Luo, Z.; Cen, K. Gas-phase elemental mercury removal by CeO_2 impregnated activated coke. *Energy Fuels* **2010**, *24*, 5426−5431.

(22) Wang, J.; Yang, J.; Liu, Z. Gas-phase elemental mercury capture by a V_2O_5/AC catalyst. *Fuel Process. Technol.* **2010**, *91*, 676−680.

(23) Xie, Y.; Li, C.; Zhao, L.; Zhang, J.; Zeng, G.; Zhang, X.; Zhang, W.; Tao, S. Experimental study on Hg^0 removal from flue gas over columnar MnO_x-CeO_2/activated coke. *Appl. Surf. Sci.* **2015**, *333*, 59−67.

(24) Tao, S.; Li, C.; Fan, X.; Zeng, G.; Lu, P.; Zhang, X.; Wen, Q.; Zhao, W.; Luo, D.; Fan, C. Activated coke impregnated with cerium chloride used for elemental mercury removal from simulated flue gas. *Chem. Eng. J.* **2012**, *210*, 547−556.

(25) Reddy, B. M.; Khan, A.; Yamada, Y.; Kobayashi, T.; Loridant, S.; Volta, J.-C. Structural characterization of CeO_2-TiO_2 and V_2O_5/CeO_2-TiO_2 catalysts by Raman and XPS techniques. *J. Phys. Chem. B* **2003**, *107*, 5162−5167.

(26) Wen, X.; Li, C.; Fan, X.; Gao, H.; Zhang, W.; Chen, L.; Zeng, G.; Zhao, Y. Experimental study of gaseous elemental mercury removal with CeO_2/γ-Al_2O_3. *Energy Fuels* **2011**, *25*, 2939−2944.

(27) Imamura, S.; Shono, M.; Okamoto, N.; Hamada, A.; Ishida, S. Effect of cerium on the mobility of oxygen on manganese oxides. *Appl. Catal., A* **1996**, *142*, 279−288.

(28) Mei, Z.; Shen, Z.; Zhao, Q.; Wang, W.; Zhang, Y. Removal and recovery of gas-phase element mercury by metal oxide-loaded activated carbon. *J. Hazard. Mater.* **2008**, *152*, 721−729.

(29) Liu, Y.; Wang, Y.; Wang, H.; Wu, Z. Catalytic oxidation of gas-phase mercury over Co/TiO_2 catalysts prepared by sol−gel method. *Catal. Commun.* **2011**, *12*, 1291−1294.

(30) Zhang, A.; Zheng, W.; Song, J.; Hu, S.; Liu, Z.; Xiang, J. Cobalt manganese oxides modified titania catalysts for oxidation of elemental mercury at low flue gas temperature. *Chem. Eng. J.* **2014**, *236*, 29−38.

(31) Xu, X.; Li, J.; Hao, Z. CeO_2-Co_3O_4 Catalysts for CO Oxidation. *J. Rare Earths* **2006**, *24*, 172−176.

(32) Bao, T.; Zhao, Z.; Dai, Y.; Lin, X.; Jin, R.; Wang, G.; Muhammad, T. Supported Co_3O_4-CeO_2 catalysts on modified activated carbon for CO preferential oxidation in H_2-rich gases. *Appl. Catal., B* **2012**, *119−120*, 62−73.

(33) Luo, J. Y.; Meng, M.; Li, X.; Li, X.-G.; Zha, Y.-Q.; Hu, T. D.; Xie, Y. N.; Zhang, J. Mesoporous Co_3O_4−CeO_2 and Pd/Co_3O_4−CeO_2 catalysts: Synthesis, characterization and mechanistic study of their catalytic properties for low-temperature CO oxidation. *J. Catal.* **2008**, *254*, 310−324.

(34) Liotta, L. F.; Di Carlo, G.; Pantaleo, G.; Venezia, A. M.; Deganello, G. Co_3O_4/CeO_2 composite oxides for methane emissions abatement: Relationship between Co_3O_4−CeO_2 interaction and catalytic activity. *Appl. Catal., B* **2006**, *66*, 217−227.

(35) Li, H.; Lu, G.; Qiao, D.; Wang, Y.; Guo, Y.; Guo, Y. Catalytic Methane Combustion over Co_3O_4/CeO_2 Composite Oxides Prepared by Modified Citrate Sol−Gel Method. *Catal. Lett.* **2011**, *141*, 452−458.

(36) Xue, L.; Zhang, C.; He, H.; Teraoka, Y. Catalytic decomposition of N_2O over CeO_2 promoted Co_3O_4 spinel catalyst. *Appl. Catal., B* **2007**, *75*, 167−174.

(37) Qu, L.; Li, C.; Zeng, G.; Zhang, M.; Fu, M.; Ma, J.; Zhan, F.; Luo, D. Support modification for improving the performance of MnO_x−CeO_y/γ-Al_2O_3 in selective catalytic reduction of NO by NH_3. *Chem. Eng. J.* **2014**, *242*, 76−85.

(38) Ranjith, K. S.; Saravanan, P.; Chen, S. H.; Dong, C. L.; Chen, C. L.; Chen, S. Y.; Asokan, K.; Rajendra Kumar, R. T. Enhanced room-temperature ferromagnetism on Co-doped CeO_2 nanoparticles: Mechanism and electronic and optical properties. *J. Phys. Chem. C* **2014**, *118*, 27039−27047.

(39) Brunel, D.; Blanc, A. C.; Garrone, E.; Onida, B.; Rocchia, M.; Nagy, J. B.; Macquarrie, D. J. Spectroscopic studies on aminopropyl-containing micelle templated silicas. Comparison of grafted and co-condensation routes. *Stud. Surf. Sci. Catal.* **2002**, *142*, 1395−1402.

(40) Wang, Y.; Yin, W. Chemical modification for PAN fibers during heat-treatment process. *Phys. Procedia* **2011**, *18*, 202−205.

(41) Gómez-Serrano, V.; Piriz-Almeida, F.; Durán-Valle, C. J.; Pastor-Villegas, J. Formation of oxygen structures by air activation. A study by FT-IR spectroscopy. *Carbon* **1999**, *37*, 1517−1528.

DOI: 10.1021/acs.energyfuels.5b00871
Energy Fuels 2015, 29, 6747−6757

(42) Li, J.; Yan, N.; Qu, Z.; Qiao, S.; Yang, S.; Guo, Y.; Liu, P.; Jia, J. Catalytic oxidation of elemental mercury over the modified catalyst Mn/α-Al_2O_3 at lower temperatures. *Environ. Sci. Technol.* **2010**, *44*, 426−431.
(43) Shan, W.; Liu, F.; He, H.; Shi, X.; Zhang, C. A superior Ce-W-Ti mixed oxide catalyst for the selective catalytic reduction of NO_x with NH_3. *Appl. Catal., B* **2012**, *115*−*116*, 100−106.
(44) Li, H.; Wu, C. Y.; Li, Y.; Zhang, J. Superior activity of MnO_x-CeO_2/TiO_2 catalyst for catalytic oxidation of elemental mercury at low flue gas temperatures. *Appl. Catal., B* **2012**, *111*−*112*, 381−388.
(45) Mei, Z.; Shen, Z.; Wang, W.; Zhang, Y. Novel sorbents of non-metal-doped spinel Co_3O_4 for the removal of gas-phase elemental mercury. *Environ. Sci. Technol.* **2008**, *42*, 590−595.
(46) Zhang, J.; Müller, J.; Zheng, W.; Wang, D.; Su, D.; Schlögl, R. Individual Fe-Co alloy nanoparticles on carbon nanotubes: Structural and catalytic properties. *Nano Lett.* **2008**, *8*, 2738−2743.
(47) Kang, M.; Song, M. W.; Lee, C. H. Catalytic carbon monoxide oxidation over CoO_x/CeO_2 composite catalysts. *Appl. Catal. A: Gen.* **2003**, *251*, 143−156.
(48) Ding, R.; Lv, L. L.; Qi, L.; Jia, M. J.; Wang, H. Y. A facile hard-templating synthesis of mesoporous spinel $CoFe_2O_4$ nanostructures as promising electrocatalysts for the H_2O_2 reduction reaction. *RSC Adv.* **2014**, *4*, 1754−1760.
(49) Liu, S. Y.; Feng, Q. G. Solid-phase synthesis and photocatalytic property of cobalt-doped TiO_2 mesoporous materials. *Adv. Mater. Res.* **2011**, *217*, 1462−1468.
(50) Mullins, D. R.; Overbury, S. H.; Huntley, D. R. Electron spectroscopy of single crystal and polycrystalline cerium oxide surfaces. *Surf. Sci.* **1998**, *409*, 307−319.
(51) Liu, X.; Zhou, K.; Wang, L.; Wang, B.; Li, Y. Oxygen vacancy clusters promoting reducibility and activity of ceria nanorods. *J. Am. Chem. Soc.* **2009**, *131*, 3140−3141.
(52) Rumayor, M.; Diaz-Somoano, M.; Lopez-Anton, M. A.; Martinez-Tarazona, M. R. Mercury compounds characterization by thermal desorption. *Talanta* **2013**, *114*, 318−322.
(53) Pitoniak, E.; Wu, C. Y.; Mazyck, D. W.; Powers, K. W.; Sigmund, W. Adsorption enhancement mechanisms of silica-titania nanocomposites for elemental mercury vapor removal. *Environ. Sci. Technol.* **2005**, *39*, 1269−1274.
(54) Zhang, H.; Zhao, J.; Fang, Y.; Huang, J.; Wang, Y. Catalytic oxidation and stabilized adsorption of elemental mercury from coal-derived fuel gas. *Energy Fuels* **2012**, *26*, 1629−1637.
(55) Kim, M. H.; Ham, S. W.; Lee, J.-B. Oxidation of gaseous elemental mercury by hydrochloric acid over $CuCl_2$/TiO_2-based catalysts in SCR process. *Appl. Catal., B* **2010**, *99*, 272−278.
(56) Granite, E. J.; Pennline, H. W.; Hargis, R. A. Novel sorbents for mercury removal from flue gas. *Ind. Eng. Chem. Res.* **2000**, *39*, 1020−1029.
(57) Yang, J.; Zhao, Y.; Zhang, J.; Zheng, C. Regenerable cobalt oxide loaded magnetosphere catalyst from fly ash for mercury removal in coal combustion flue gas. *Environ. Sci. Technol.* **2014**, *48*, 14837−14843.
(58) Presto, A. A.; Granite, E. J. Survey of catalysts for oxidation of mercury in flue gas. *Environ. Sci. Technol.* **2006**, *40*, 5601−5609.
(59) Grabowski, R.; Pietrzyk, S.; Słoczyński, J.; Genser, F.; Wcisło, K.; Grzybowska-Świerkosz, B. Kinetics of the propane oxidative dehydrogenation on vanadia/titania catalysts from steady-state and transient experiments. *Appl. Catal., A* **2002**, *232*, 277−288.
(60) Jin, R.; Liu, Y.; Wu, Z.; Wang, H.; Gu, T. Low-temperature selective catalytic reduction of NO with NH_3 over MnCe oxides supported on TiO_2 and Al_2O_3: A comparative study. *Chemosphere* **2010**, *78*, 1160−1166.
(61) Fuente-Cuesta, A.; Lopez-Anton, M. A.; Diaz-Somoano, M.; Martínez-Tarazona, M. R. Retention of mercury by low-cost sorbents: Influence of flue gas composition and fly ash occurrence. *Chem. Eng. J.* **2012**, *213*, 16−21.
(62) Li, Y.; Murphy, P. D.; Wu, C.-Y.; Powers, K. W.; Bonzongo, J.-C. J. Development of Silica/Vanadia/Titania catalysts for removal of elemental mercury from coal-combustion flue gas. *Environ. Sci. Technol.* **2008**, *42*, 5304−5309.
(63) Oza, T.; Jha, J.; Ezekiel, E. Thermal decomposition of barium- and mercury (2) nitrate. *J. Indian Chem. Soc.* **1968**, *45*, 420−424.
(64) Guo, Y.; Yan, N.; Yang, S.; Liu, P.; Wang, J.; Qu, Z.; Jia, J. Conversion of elemental mercury with a novel membrane catalytic system at low temperature. *J. Hazard. Mater.* **2012**, *213-214*, 62−70.
(65) Li, H.; Wu, C. Y.; Li, Y.; Zhang, J. CeO_2-TiO_2 catalysts for catalytic oxidation of elemental mercury in low-rank coal combustion flue gas. *Environ. Sci. Technol.* **2011**, *45*, 7394−7400.
(66) Tan, Z.; Su, S.; Qiu, J.; Kong, F.; Wang, Z.; Hao, F.; Xiang, J. Preparation and characterization of Fe_2O_3-SiO_2 composite and its effect on elemental mercury removal. *Chem. Eng. J.* **2012**, *195*−*196*, 218−225.
(67) Li, Y.; Wu, C.-Y. Role of moisture in adsorption, photocatalytic oxidation, and reemission of elemental mercury on a SiO_2-TiO_2 nanocomposite. *Environ. Sci. Technol.* **2006**, *40*, 6444−6448.
(68) Huang, Y.; Gao, D.; Tong, Z.; Zhang, J.; Luo, H. Oxidation of NO over cobalt oxide supported on mesoporous silica. *J. Nat. Gas Chem.* **2009**, *18*, 421−428.

DOI: 10.1021/acs.energyfuels.5b00871
Energy Fuels 2015, 29, 6747−6757